tvst

https://doi.org/10.1167/tvst.8.4.28

Article

Distance-Thresholded Intercapillary Area Analysis Versus Vessel-Based Approaches to Quantify Retinal Ischemia in OCTA

Peer Lauermann[1], Christian van Oterendorp[1], Marcus W. Storch[1], Mohammed H. Khattab[1], Nicolas Feltgen[1], Hans Hoerauf[1], and Sebastian Bemme[1]

[1] Department of Ophthalmology, University Medical Center Göttingen, Göttingen, Germany

Correspondence: Sebastian Bemme, Department of Ophthalmology, University Medical Center Göttingen, Robert-Koch-Straße 40, 37075 Göttingen, Germany. email: sebastian.bemme@med.uni-goettingen.de

Received: 10 January 2019
Accepted: 4 June 2019
Published: 19 August 2019

Keywords: OCT-angiography; ischemia; retina

Citation: Lauermann P, van Oterendorp C, Storch MW, Khattab MH, Feltgen N, Hoerauf H, Bemme S. Distance-thresholded intercapillary area analysis versus vessel-based approaches to quantify retinal ischemia in OCTA. Trans Vis Sci Tech. 2019;8(4):28, https://doi.org/10.1167/tvst.8.4.28

Purpose: To develop and compare different analytic approaches for quantifying ischemia in OCT-angiography (OCTA), including vessel-based approaches and intercapillary area analysis.

Methods: En face OCTA (6 × 6) images of the superficial plexus of 20 healthy eyes and 20 eyes with different ischemic retinal diseases were analyzed retrospectively. Included retinal diseases were diabetic retinopathy ($n = 9$), central ($n = 5$) and branch retinal vein occlusion ($n = 4$), hypertensive retinopathy ($n = 1$), and occlusive retinal vasculitis in sarcoidosis ($n = 1$). Vessel-based approaches consisted of the mean gray scale, perfusion density, and vessel density. Intercapillary areas (ICAs) were analyzed measuring the distance of each intercapillary pixel from the surrounding vessels. In particular, we applied a vector method to measure the shortest, the mean, and the longest distance in eight predefined directions. Size of ICAs was determined applying different global or local distance thresholds.

Results: All approaches revealed significant differences between ischemic and healthy retinae ($P < 0.001$, with Bonferroni-Holm correction $P = 0.001$–0.025; Wilcoxon-Mann-Whitney test). Discrimination between the healthy and ischemic retinae based on ROC curves was best in the ICA analysis using a locally set threshold of the shortest distance.

Conclusions: In the present study, ICA analysis was superior to vessel-based approaches in the quantification of retinal ischemia when defining a local or global distance threshold.

Translational Relevance: In order to establish OCTA imaging in everyday clinical and scientific practice, standardized, device-independent image analysis methods are necessary.

Introduction

Central retina ischemia is the consequence of several retinal diseases such as diabetic retinopathy and venous or arterial retinal circulatory disorders. Although fluorescence angiography is currently the gold standard for assessing the degree of ischemia, it has several shortcomings, such as the lack of an established, objective ischemia-quantification system usable in the daily routine,[1–4] the 2D-image limitation,[5] and the invasiveness of intravenous dye application.[6]

OCT-angiography (OCTA) allows the retinal and choroidal vasculature to be visualized in just a few seconds and without requiring dye injection.[7] Various recent studies attempted to quantify vascular alterations using OCTA. One part of them used commercially available built-in algorithms for image analysis,[8–13] and others used different self-developed algorithms.[14–16] Frequently used approaches were to measure the area of the foveolar avascular zone (FAZ), measure vessel density, and measure perfusion density.[8–11,14,15,17] Both perfusion density and vessel density are reported as a percentage of the

vascularized areas relative to the total area of the OCTA image. In contrast to perfusion density, vessel density relies on a skeletonized image of the retinal blood vessels.

Recently, approaches to quantify retinal ischemia by analyzing the intercapillary areas (ICAs) have been reported. Zhang et al.[16] developed a vessel distance map for each OCTA image where each pixel's distance to the nearest vessel is given. Schottenhamml et al.[18] introduced a method that analyzes the sizes of ICAs.

All the aforementioned methods have different limitations. The FAZ revealed significant variability, even between healthy eyes,[17] and only a small part of the OCTA image is analyzed. Larger, peripheral vessels and avascular areas are neglected, making the method unsuitable for automatic quantification of retinal ischemia caused by venous or arterial circulatory disorders. Vessel density and perfusion density require thresholding before image analysis, and their sensitivity for discrete capillary network pathologies tends to be limited.[18] ICA quantification requires numerous preprocessing steps and can lack robustness due to small vessel gaps.[13,16,18]

So far, none of these techniques have become established as a standard method for quantifying central retina ischemia, and there has been no systematic comparison of existing methods. The aim of this study was to compare different analytic algorithms for automated quantification of retinal ischemia in OCTA.

Methods

Study Population

In this retrospective study, 6 × 6-mm en face OCTA (Zeiss AngioPlex; Carl Zeiss Meditec, Dublin, CA) images of the superficial vascular plexus of 20 healthy eyes and 20 eyes with different ischemic retinal diseases were included. The study adhered to the tenets of the Declaration of Helsinki and was approved by our local ethics committee. OCTA images of ischemic eyes were selected after a database research of the AngioPlex device by two trained investigators (PL and SB) who had at least 2 years of clinical experience in analyzing OCTA scans.

Inclusion criteria for ischemic retinae required clear visible areas of nonperfusion and the diagnosis of a vascular retinopathy typically causing retinal vessel loss. Control retinae were defined as having intact retinal microvasculature with absence of any vessel dropout. We included only healthy subjects without history of diabetes. A minimum age of 18 years was defined for all included patients and controls. Furthermore, only images with a signal strength ≥6/10 were included in this study.

OCTA Imaging

The AngioPlex OCTA device works with a 68-kHz spectral domain-OCT scanner with a center wavelength of 840 nm and uses the optical microangiography-complex (OMAG^c) algorithm. The algorithm analyzes the change in complex signal and then generates en face microvascular images measuring 6 × 6 mm.

The AngioPlex device automatically determines the superficial retinal vascular slab by detecting the internal limiting membrane and inner plexiform layer as their boundaries.[19–21] Correct segmentation of the layers was confirmed by reviewing all overlaid OCTA B scans by two graders (PL and SB). Subsequently, en face images were exported in TIFF format for further analysis.

Contrast Normalization and Binarization

Prior to image analysis, contrast normalization across all OCTA images was conducted using a two-step algorithm. Firstly, gray values of all pixels were shifted by the difference between the mean gray value of the 5% darkest pixel and the same parameter of a reference image. Secondly, gray values of all pixels were multiplied by the ratio of the mean gray value of the 5% brightest pixels and the same parameter of the reference image. An OCTA image from the control group revealing good visual discrimination between capillaries and ICA served as reference. For further analysis (methods 2–8), binarized images were used. Binarization categorized all pixels as vessel and nonvessel pixels. For all images, a pixel intensity threshold of 50 (8 bit) was applied (see Fig. 1, B1 and B2).

Image Analysis

Images were analyzed using self-developed scripts (MATLAB; MathWorks, Natick, MA). Different analytic approaches were applied to each OCTA image, including vessel analysis and ICA analysis.

Vessel-Based Methods

Methods included (1) mean gray value, (2) perfusion density, and (3) vessel density. Perfusion

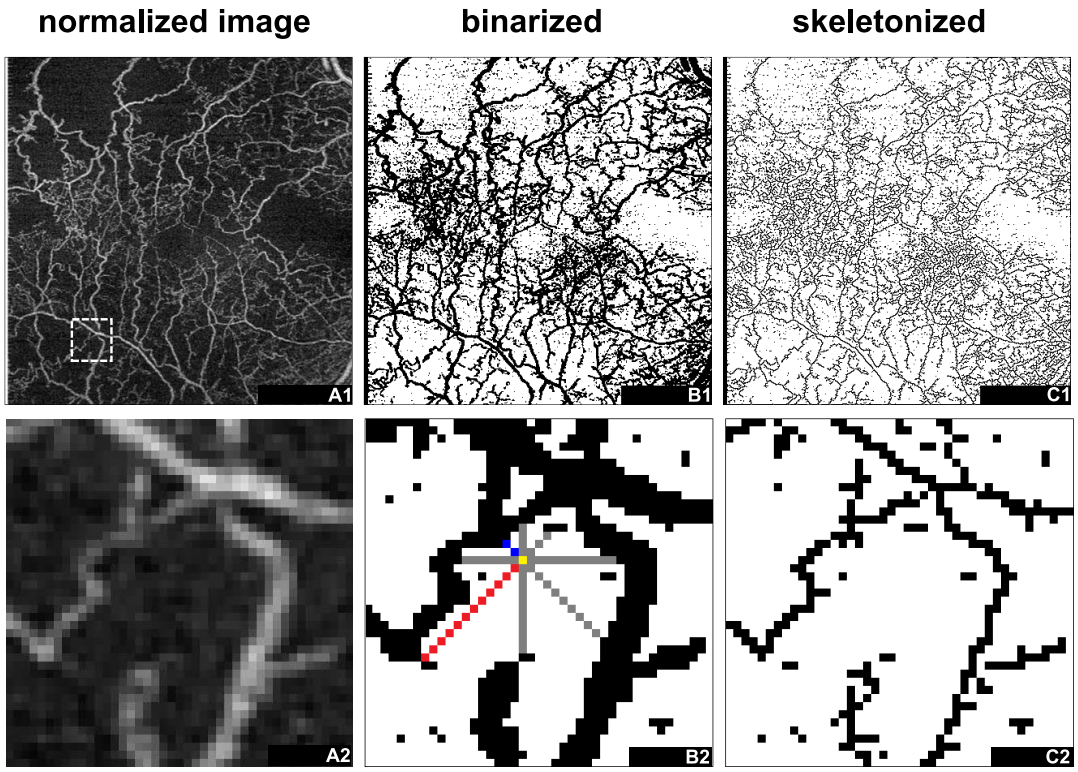

Figure 1. Image analysis, different preprocessing methods, and visualization of the distance (vector) approach. Top row with en face OCTA images in original size: (A1) original image; (B1) binarized image; (C1) skeletonized image. Bottom row with magnified images of the region of interest (indicated by the *dashed frame* in A1) in all top row images; (B2) with additional visualization of the distance (vector) approach, shortest vector *blue*, longest vector *red*, pixel of interest *yellow*.

density was calculated as percentage of all vessel pixels on the image area. Vessel density of the total blood vessel length was based on a skeletonize algorithm as percentage on the image area. The skeletonize algorithm was applied before binarization and detected the lowest gray scale in a 2 × 2-pixel square kernel and eliminated the pixel with the lowest gray value, resulting in skeletonized vessels with a width of 1 pixel (see Fig. 1, C1 and C2).

Distance-Thresholded Analysis of the ICAs

Size of areas between vessels were determined as described by Schottenhamml et al.[18] To do so, nonvessel pixels from binarized images directly connected to each other in the x or y direction were assigned to one individual ICA. To apply the distance approach, only pixels with a distance to the surrounding vessels above a fixed or local varying threshold were analyzed. The size of each area was determined as the number of pixels. The cumulative distance-thresholded ICA (equals the sum of all individual ICAs) as well as the average size of the 10 and 20 largest ICAs were calculated for each OCTA image. In detail, methods of intercapillary area analysis contained the (4a to c) sum of all ICAs with fixed distance threshold; (5a to c) sum of all ICAs with local distance threshold; (6) mean of the 10 and 20 largest ICAs without distance threshold; (7a to c) mean of the 10 and 20 largest ICAs with fixed distance threshold; and (8a to c) mean of the 10 and 20 largest ICAs with local distance threshold.

The distance to the surrounding vessels was assessed via a vector method, where from each nonvessel pixel the length of a vector to the next blood vessel was measured. From each pixel, eight vectors in eight preset directions were drawn (see Fig. 1, B2). Each vector's length was determined as the distance between the analyzed pixel and the nearest blood vessel. This approach contained three subgroups: the shortest vector to the next blood vessel (SV), the mean length of all vectors originating from this pixel (MV), and the longest vector to the next blood vessel (LV). For each subgroup, only pixels with vectors above a given vector length (fixed distance threshold) were counted: SV $>$ 2, MV $>$ 6, and LV $>$ 14 pixels. The respective threshold values

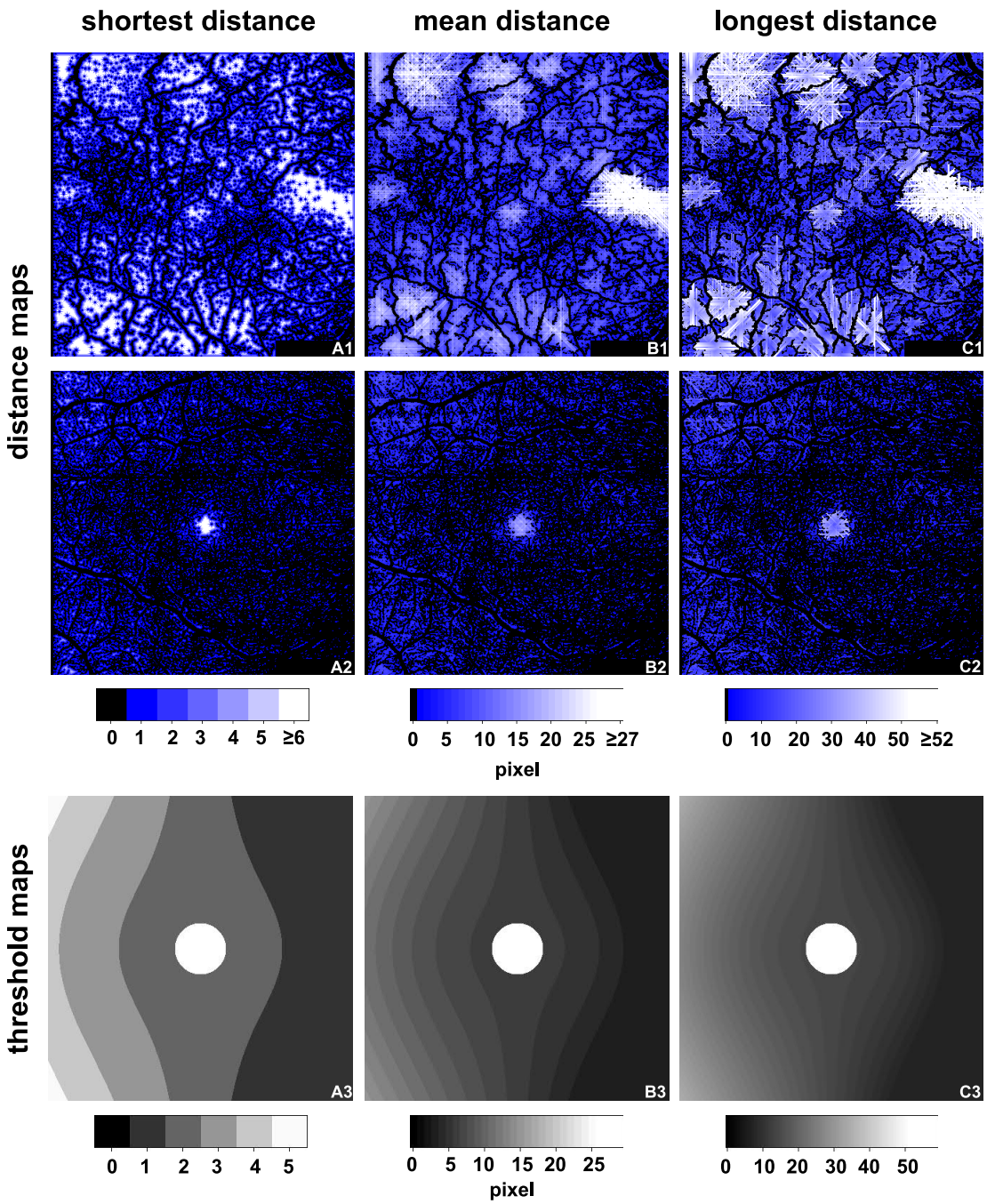

Figure 2. Color-coded distance maps derived from the vector length in ischemic (A1 to C1) and healthy retina (A2 to C2). Threshold maps (A3 to C3) of local distance threshold DT(x′y′) were obtained by setting the same values that had been used as fixed distance thresholds as paracentral baseline threshold value (DT_M) and empirically modulating it according to the x/y position by Equation 3. The range of thresholds shown outside the center was 1 to 5 (SV), 3 to 15 (MV), and 7 to 35 (LV).

were determined from previous independent analyses. Figure 2 shows vector length (or distance) maps for ischemic (top row) or healthy (bottom row) retinae.

We further applied a local distance threshold based on a threshold map instead of a globally fixed value. Since the inferior temporal and superior temporal capillary network is physiologically less dense than the parafoveal and nasal vasculature, we defined a local distance threshold DT($x'y'$) dependent on the

Table 1. Study and Control Population, Baseline Characteristics

	Patients/ Eyes, No.	Mean Age	Sex	Mean Signal Strength	Mean Visual Acuity	Retinal Diseases (No. of eyes)
Retinal ischemia group	19/20	57.85 y	12 male, 7 female	8.5 of 10	0.52	Diabetic retinopathy (9) Central retinal vein occlusion (5) Branch retinal vein occlusion (4) Hypertensive retinopathy (1) Occlusive retinal vasculitis (1)
Control group	17/20	57.10 y	12 male, 5 female	8.95 of 10		

relative distance to the vertical line through the fovea,

$$d_M = \frac{215 - x'}{214}, \quad (1)$$

and dependent on the relative distance to the fovea,

$$d_F = \sqrt{\frac{0.5 \times (215 - x')^2 + (215 - y')^2}{1.5 \times 214^2}}, \quad (2)$$

with

$$\mathrm{DT}(x'y') = \mathrm{DT}_M + 1.5 \times \mathrm{DT}_M \times d_M \times d_F. \quad (3)$$

DT_M, representing the baseline distance threshold around the fovea, was set to SV = 2, MV = 6, and LV = 14, which were the same values that had been used as fixed distance thresholds (method 4). Minimal DT was set to $\mathrm{DT}_M \times 0.5$. To exclude pixels of a physiological, that is nonenlarged, FAZ from analysis, the distance threshold of all pixels within a radius 0.5 mm from the fovea (which equals the center of an EDTRS grid) was set to SV = 36, MV = 36, and LV = 72, respectively. Figure 2 displays the resulting threshold maps for the shortest vector (A3), mean of vectors (B3), and the longest vector (C3).

Statistics

Statistical analysis was performed using software (GraphPad PRISM 6; GraphPad Software, La Jolla, CA). Bonferroni-Holm correction for multiple comparison was applied. Differences between healthy and ischemic eyes for each approach were analyzed using the Wilcoxon-Mann-Whitney test. The area under the receiver operating characteristic curve–area under the ROC curve (ROC-AUC) was calculated for each approach. P values <0.05 were considered significant.

Results

Baseline Characteristics

The retinal ischemia group presented different causes of microvascular disease: diabetic retinopathy ($n = 9$), central ($n = 5$) and branch retinal vein occlusion ($n = 4$), hypertensive retinopathy ($n = 1$), and occlusive retinal vasculitis in sarcoidosis ($n = 1$). Further baseline characteristics of the retinal ischemia and the control group are provided in Table 1. There was no significant difference in the mean age between both groups ($P = 0.881$, mean ± SEM ischemic/control: 57.85 ± 3.42 years/57.1 ± 3.59 years), image quality ($P = 0.337$, mean ± SD ischemic/control: 8.5 ± 1.4/8.95 ± 0.76), and sex distribution ($P > 0.999$).

Discrimination Between Healthy and Ischemic Retinae via Vessel-Based Image Analysis (Methods 1–3)

Using unpaired t-tests for each approach, all approaches showed significant differences between healthy and ischemic retinae ($P = 0.001$–0.025) displayed by Figures 3 and 4. For detailed information on test statistics, see Tables 2, 3, and 4. Among the vessel-based analyses (methods 1–3), vessel density (method 3) revealed the highest ROC-AUC (AUC = 0.94), followed by perfusion density (method 2: AUC = 0.8975). The mean gray value (method 1) showed the lowest ROC-AUC (AUC = 0.8825).

Discrimination Between Healthy and Ischemic Retinae via the Cumulative ICA (Methods 4 and 5)

First, ICA analysis was performed with fixed distance thresholds (methods 4a–4c), which were

Table 2. Mean ± SEM and ROC-AUC of Mean Gray Value (Method 1), Perfusion Density (Method 2), and Vessel Density (Method 3)

	Mean Gray Value, Method 1	Perfusion Density, Method 2	Vessel Density, Method 3
Mean ± SEM			
Ischemic	60.57 ± 1.285	54.39% ± 2.202%	29.21% ± 0.951%
Control	68.37 ± 0.611	69.05% ± 1.031%	35.61% ± 0.413%
ROC-AUC	0.8825	0.8975	0.94

obtained from preliminary experiments. Here, the SV subgroup (method 4a: AUC = 0.95) was superior to the MV (method 4b: AUC = 0.9425) and LV (method 4c: AUC = 0.9375) approaches. Replacing the fixed distance threshold by local threshold maps increased the ROC-AUC of only the SV approach (methods 5a). Here again, the SV approach performed better than the other approaches (method 5a: AUC = 0.96; method 5b: AUC = 0.9225; method 5c: AUC = 0.9325).

ROC-AUC for perfusion density (method 2) and the cumulative ICA with SV >0 (data not shown) displayed the same value (AUC = 0.8975). This is attributable to the fact that defining the vector threshold of >0 creates an inverted image of the binarized image. Moreover, this demonstrates that the vector method reliably detected avascular areas and avoids vessels.

Discrimination Between Healthy and Ischemic Retinae Analyzing the Largest ICAs (Methods 6–8)

Averaging the 10 and 20 largest ICAs as determined by the most straightforward method (method 6) resulted in ROC-AUC at the lower end (10 largest ICAs: AUC = 0.915; 20 largest ICAs: AUC = 0.9175). Combining method 6 with a fixed or local distance threshold (method 7 and 8) resulted in markedly higher ROC-AUC.

Compared to cumulative analysis, focusing only on the 10 and 20 largest ICAs showed similar discrimination between healthy and ischemic retinae using the MV (method 7b: AUC = 0.94 and AUC = 0.9425) and the LV (method 7c: AUC = 0.9325 and AUC = 0.9325) approaches with fixed distance thresholds. However, discrimination decreased, averaging only the largest ICAs for the SV approach with a fixed distance threshold (method 7a: AUC = 0.9175 and AUC = 0.9375 versus method 4a: AUC = 0.95).

Analogue to the superiority of method 5a over method 4a, the application of local distance thresholds for the SV approach (method 8a) further increased the discrimination compared to the shortest distance with a fixed threshold (method 7a).

Comparison of ICAs Depending on the Applied Distance Threshold

Figure 5 displays OCTA images of healthy and ischemic retinae with ICAs color-coded depending on the size of the individual area. Calculating ICA simply from all nonvessel pixels (method 6) detected the complete area between the vessels (Fig. 5, A1 and A2).

Table 3. Mean ± SEM and ROC-AUC of the Cumulative ICA of Pixels With a Shortest Vector (SV), a Mean Vector Length (MV), and a Longest Vector (LV) to the Surrounding Vessels Above a Fixed Distance Threshold (Methods 4a to 4c) or a Local Distance Threshold (Methods 5a to 5c)

	Fixed Distance Threshold (Method No.)			Local Distance Threshold (Method No.)		
	SV > 2 (4a)	MV > 6 (4b)	LV > 14 (4c)	SV (5a)	MV (5b)	LV (5c)
Mean ± SEM of area, pixel						
Ischemic	17,535 ± 2,825	27,242 ± 4,416	29,730 ± 4,506	13,602 ± 2,584	24,345 ± 4,469	26,999 ± 4,601
Control	3,422 ± 392.4	4,127 ± 642.7	5,438 ± 765.2	1,264 ± 229.6	1,795 ± 503	2,712 ± 578.9
ROC-AUC	0.95	0.9425	0.9375	0.96	0.9225	0.9325

Applying a local distance threshold based on the threshold maps, shown in Figure 2, A3 to C3, to the vector analysis increased the discrimination between ischemic and control retinae only for the SV. Overall, the approach 5a (SV with local distance threshold) had the highest ROC-AUC.

Table 4. ROC-AUC for the Approaches Averaging the Size of the 10 and 20 Largest ICAs

	Fixed Distance Threshold (Method No.)			
	SV > 0 (6)	SV > 2 (7a)	MV > 6 (7b)	LV > 14 (7c)
Mean ± SEM of area, pixel				
10 largest ICAs				
Ischemic	3977 ± 466.3	992.6 ± 219.9	2203 ± 376.1	2257 ± 383.2
Control	1331 ± 148.4	164.7 ± 14.61	337.8 ± 43.68	352 ± 46.77
20 largest ICAs				
Ischemic	2312 ± 247.1	570.2 ± 119	1203 ± 198.9	1222 ± 202
Control	830.2 ± 89.01	93.89 ± 7.24	179.4 ± 24.99	189.7 ± 25.78
ROC-AUC				
10 largest ICAs	0.915	0.9175	0.94	0.9325
20 largest ICAs	0.9175	0.9375	0.9425	0.9325

Table 4. Extended

	Local Distance Threshold (Method No.)		
	SV (8a)	MV (8b)	LV (8c)
Mean ± SEM of area, pixel			
10 largest ICAs			
Ischemic	722.7 ± 186.7	1810 ± 377.7	1898 ± 386.6
Control	32.97 ± 6.287	104.3 ± 27.04	104 ± 25.58
20 largest ICAs			
Ischemic	414.7 ± 100.5	1004 ± 199.3	1043 ± 203.9
Control	22.58 ± 3.838	63.26 ± 16.25	63.77 ± 15.19
ROC-AUC			
10 largest ICAs	0.9575	0.935	0.9425
20 largest ICAs	0.955	0.935	0.94

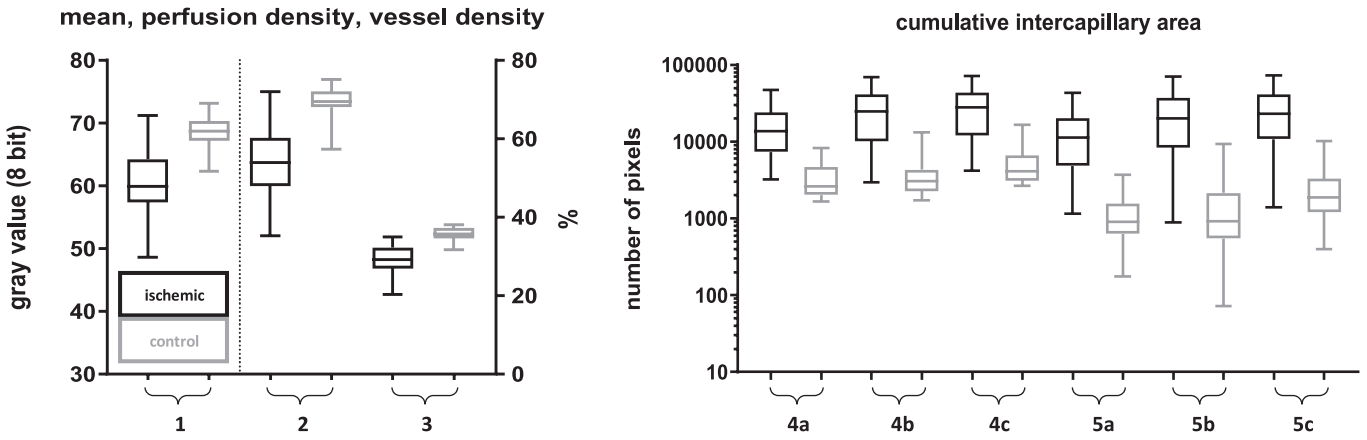

Figure 3. Plotted data of the approaches 1 to 5. All approaches exhibited significant differences between healthy (control, *gray*) and ischemic (patients, *black*) eyes with $P < 0.001$ (after Bonferroni-Holm correction, $P = 0.001$–0.011, Wilcoxon-Mann-Whitney test).

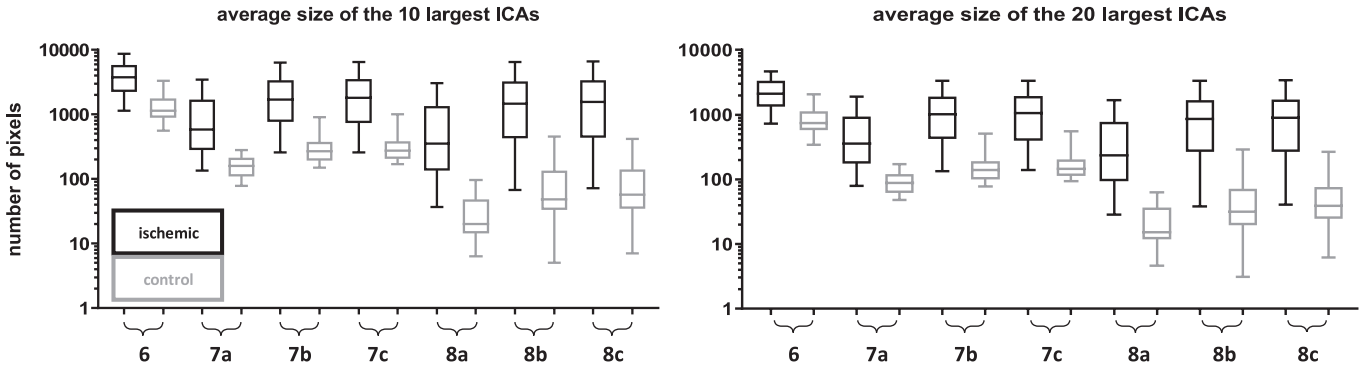

Figure 4. Average size of the 10 and 20 largest ICAs (methods 6–8c); all approaches showed significant differences between healthy and ischemic retinae ($P < 0.001$, after Bonferroni-Holm correction $P = 0.012$–0.025).

With method 6, ICAs were overproportionally larger than using the SV approach with a fixed distance threshold >2, which was due to small vessel discontinuities assigning several smaller ICAs to a bigger one, even if those are connected by only a 1-pixel-wide vessel gap. This also led to the false-positive detection of ischemic zones in healthy retinae (see temporal superior part of OCTA image, Fig. 5, A2). Applying a fixed distance threshold of >2 markedly reduced this false-positive detection of ischemic areas in healthy retinae (see temporal superior part of OCTA image, Fig. 5, B2), while small avascular areas in the ischemic retina were still detected.

Since the SV approach with a fixed distance threshold of >2 excluded a thin halo around each single pixel with a gray value ≥50, an avascular area with numerous noise pixels may be cut into several smaller areas (see Fig. 5, A1 and B1: compare the largest avascular area in the superior temporal part). Both the MV and LV approaches appeared more robust against this type of artifact and displayed large avascular areas more homogenously than did the SV approach (Figs. 5, C1 and D1). However, medium-sized avascular areas appeared less homogenously (white to yellowish) with the LV approach compared to the MV method.

Combined with local distance threshold maps, the FAZ was no longer detected as an avascular area, and more areas were determined as being avascular than with the fixed distance threshold (Fig. 5, B3–D3). Furthermore, fewer physiological ICAs were false positively detected in healthy retinae, except in the nasal part due to the lower threshold (Figure 5, B3–D3).

To test the above-mentioned observations, we compared the size of ICAs obtained by two different methods using the Bland-Altman analysis (Supplementary Fig. S1). Comparing methods 6 to 7a, 7b, and 7c confirmed that sizes of ICAs were detected as being overproportionally larger by method 6. A systematic detection of larger ICAs by method 6 compared to method 7a was expected due to the applied distance threshold, but that did not explain a ratio up to 2^{10} for healthy retinae. Furthermore, Bland-Altman analysis confirmed that ICAs were detected as being larger with the MV and the LV method compared to the method with shortest distance threshold >2, which seems to be the converse for small ICAs. Regarding methods 7a versus 8a, 7b versus 8b, and 7c versus 8c, separate comparison of ICA sizes in the nasal third and temporal third of the OCTA image by Bland-Altman plots confirmed that the detection of nonvascular areas was increased in the nasal part of the OCTA image but decreased in the region temporal to the macula via the local distance threshold.

Comparison of Ranks

Ranks of datasets were compared using the Spearman rank order correlation. Figure 6 displays a heat map of the correlation coefficients of each possible method pair. Ranks of vessel-based approaches exhibited the best correlations between methods 1 and 2 (rho = 0.97). Lower rho were found comparing methods 1 and 2 with all the other methods (rho 0.72–0.92), except with method 6 when averaging the 20 largest areas (rho = 0.94 and 0.95). In contrast, vessel density (method 3) correlated strongly with distance-based methods 4a to 5c (rho between 0.95 and 0.98), but less with methods 6 to 8c, averaging the 10 or 20 largest ICAs (rho between 0.87 and 0.96). Rank comparisons among all distance-

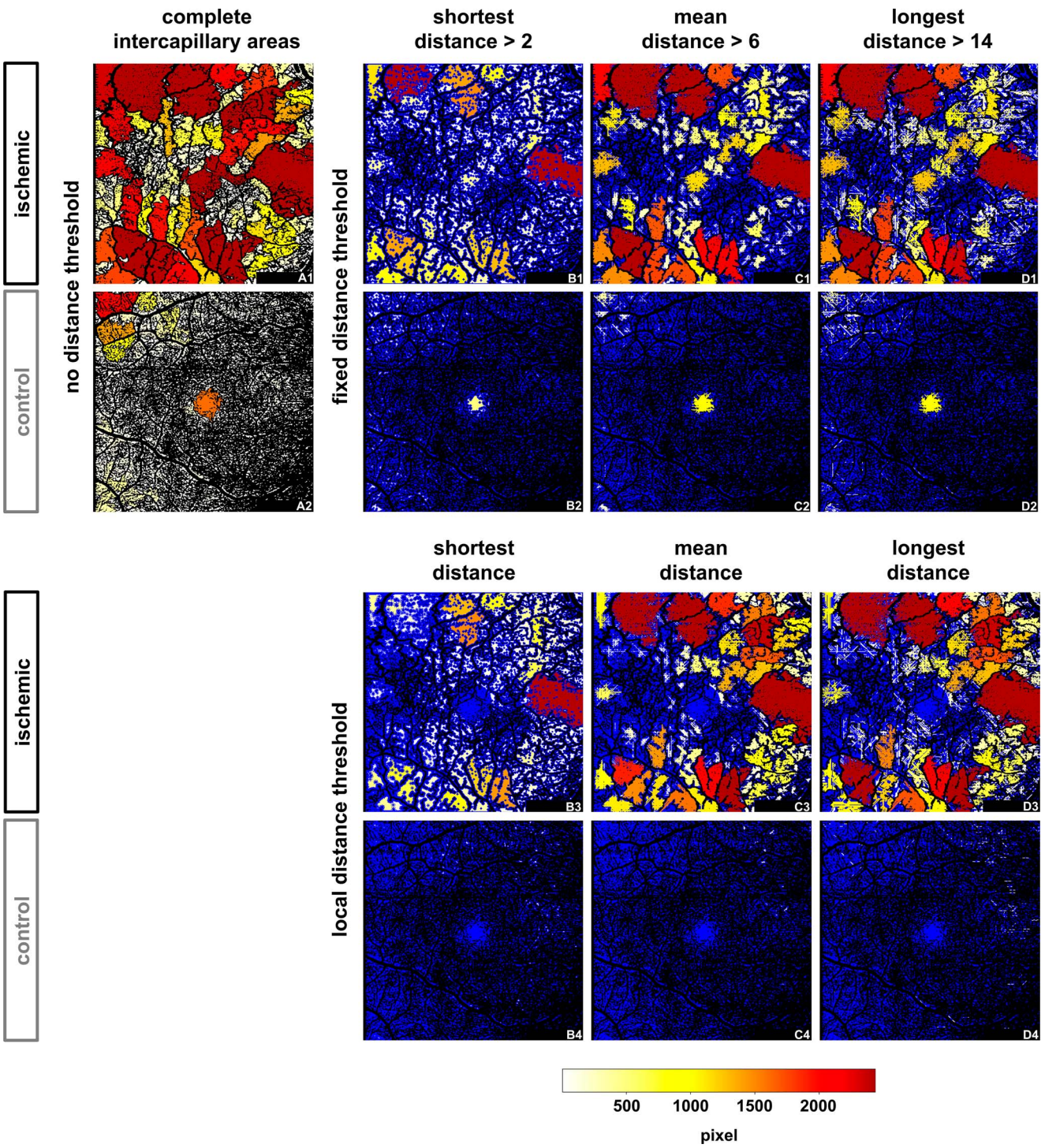

Figure 5. Visualization of ICAs depending on the applied distance threshold comparing no threshold (method 6; A1 and A2), fixed distance threshold (method 7; rows 1 and 2, B to D), and local distance threshold (method 8; row 3 and 4). The color-coded maps show areas classified as ischemic in a *white-to-red* color. The actual color on the *white-to-red* scale depends on the respective area's size in pixels. (See *legend bar* below row 4. Range from 0 to 2440. ICAs larger than 2440 pixels are displayed in the same color). Rows 1 and 3 show the same ischemic and rows 2 and 4 the same healthy retina. Images in column A display entire ICAs with their respective color-coded size (equivalent to SV $>$ 0) for an ischemic (A1) and healthy (A2) retina. Columns B, C, and D show the ICAs obtained after applying fixed (rows 1 and 2) or local (rows 3 and 4) distance thresholds for SV, MV, and LV, respectively. For the local distance thresholds DT(x′y′) displayed as threshold maps (see Fig. 2, A3 to C3), fixed thresholds with best AUC for global analysis were used as baseline threshold →

←
value (DT_M) and modulated according to their x/y position as described in the Methods section. Intercapillary pixels with distances below the threshold are shown in *blue*. While the fixed distance threshold produced false-positive (ischemic) areas in the healthy controls (B2/C2/D2; top *left* quadrant and FAZ), the local distance threshold displayed much better specificity with no obvious loss of sensitivity. In the *right* part of the images (nasally to the fovea), the sensitivity even seems increased (more *yellow* areas in ischemic retina but not in the healthy one).

based methods 4 to 5 and 7 to 8 demonstrated a strong correlation with rho between 0.95 and 1, except when compared with method 6 (rho $>$ 0.79), method 7a (rho $>$ 0.88), or method 8a (rho $>$ 0.88). Lowest rank correlation was found comparing datasets of methods 7a to method 1 (rho = 0.72 and 0.75) and 2 (rho = 0.75 and 0.78), respectively.

Summary of Results

All our approaches revealed significant differences between ischemic and healthy retinae. ($P < 0.001$, Wilcoxon-Mann-Whitney test; after Bonferroni-Holm correction, $P = 0.001$–0.025). The discrimination between healthy and ischemic was best in the distance-thresholded ICA analysis. Using locally set distance thresholds, discrimination of healthy and ischemic was improved further for the shortest distance, achieving an ROC-AUC of 0.96 (method 5a). Individual analysis of only the 10 or 20 largest ICAs did not markedly enhance the discrimination, but it did improve the visualization of ischemic areas.

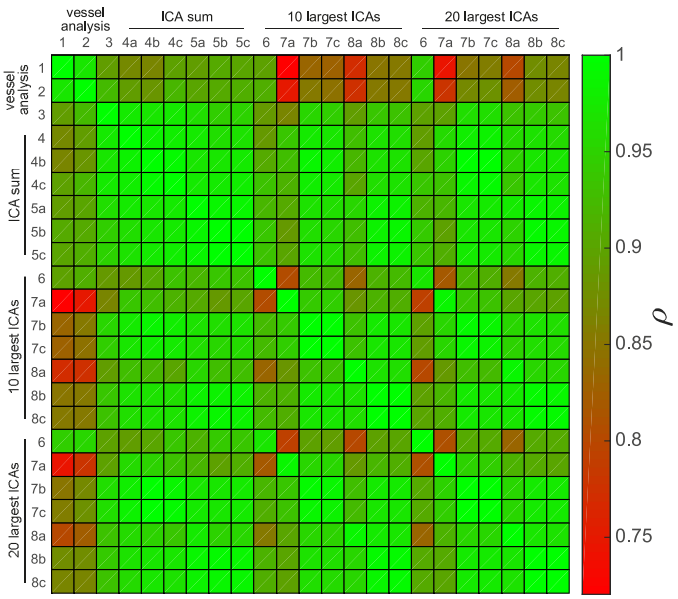

Figure 6. Heat map of Spearman rank correlation for each possible method pair with rho color-coded.

Discussion

Various methods to quantify retinal ischemia in OCTA images have been proposed. As there are no studies comparing different approaches within one population, we compared different postprocessing methods by self-developed MATLAB scripts. All of our approaches detected significant differences between healthy and ischemic retinae, but ROC analyses differed markedly in how they discriminated between healthy and ischemic vasculature. There are two basic approaches to quantify retinal ischemia in OCTA: vessel-based approaches or those focusing on avascular area detection.

Calculation of Nonvascular Area Versus Vessel-Based Methods

Vessel-based methods include measuring the perfusion density and vessel density. In the present study, vessel density was superior to the perfusion density approach. A possible explanation is that in binarized images, each vessel's width varies to a certain degree. Since vessel loss initially affects capillaries, perfusion density is less reduced than vessel density, which is calculated on skeletonized vessels brought to a 1-pixel width.

Measuring the total size of the nonvascular area is only the inverted value of the perfusion density and therefore does not improve the detection of ischemia compared to vessel-based approaches. However, focusing on individual nonvascular pixels enables analysis of individual areas: measuring the size of FAZ or the size of only a distinct number of the largest avascular areas.[18]

Mapping of local flow impairment measured by vessel-based methods requires applying a kernel of defined pixel size, which enables visualization of subtle vessel loss with high resolution.[22] However, the information about the extent of the local flow impairment is limited to the size of the kernel. In contrast, connected component analysis as introduced by Schottenhamml et al.[18] directly measures the size of the nonperfusion areas and enables quantification

and visualization of the extent of the local flow impairment. Averaging only the 10 or 20 largest ICAs may emphasize large flow-impairment zones and artificially ignore subtle vessel loss. However, it gives additional information about the maximal extent of local flow impairment and may represent a complementary analysis to the cumulative ICA or to vessel-based parameters.

In a theoretical sense, analyzing the size of individual ICAs is superior to vessel-based methods, since the loss of a single vessel affects vessel density and perfusion density measurements only a little, but the size single ICAs increase is disproportionately high when the separating vessels have disappeared and two adjacent areas become connected. Regarding the relative increase in area, this is particularly relevant for small ICAs. In our study, however, this method (method 6) was not superior to vessel-based methods due to the frequent false-positive detection of ischemic areas in healthy patients. We believe that this was mainly due to the erroneous connection of originally separated ICAs through artificial vessel gaps. A 1-pixel gap in a capillary would suffice to connect two separate areas to become one large area. This makes this method prone to false-positive results due to local contrast variations or imaging artifacts.[18] Motion artifacts, like vessel doubling, stretch artifacts, displacement, and quilting tend to occur in OCTA; these can be minimized but not eliminated using an eye tracker.[23] To improve image quality before analysis, recent studies applied a vesselness filter.[16,24] We deliberately avoided additional image processing before analysis as each image-processing step can lead to a loss of information.

Distance Approach

To overcome the aforementioned problems involving simple ICA measurements as in method 6, we modified our analysis algorithm by applying a distance threshold, measuring only nonvessel pixels with a defined distance to the next vessel. This markedly improved the discrimination between ischemic and healthy retinae. Specificity was especially improved, presumably because of the greater robustness of the vector-based approach against small vessel gaps.

Previous studies that aimed to detect avascular areas by applying a distance threshold used an Euclidean distance transform to the binary vessel mask.[16] The vector method described in our study measured the distance between "nonvessel" pixels to the next vessel in only eight directions. This may, due to the lower resolution, only approximate the shortest distance to the next vessel. However, the vector approach enables additional measurements of the mean distance and the longest distance since it considers only the surrounding vessels. All three of the distance approaches (shortest, mean, and longest) correspond with the size of the nonperfusion area. We nevertheless applied and compared the three different distance measurements as we assumed that those metrics are also dependent on the shape of the nonperfusion area and differentially prone to noise within the nonperfusion areas.

Since the vector approach measured the distance to each pixel above a defined gray value, single noise pixels located within avascular areas were also identified as vessel pixels. This might have significantly reduced the sensitivity of the SV approach for avascular area detection when those were filled with numerous single pixels above the gray value threshold, as a 2-pixel-wide area around each single "vessel-pixel" is missing. Furthermore, it explains the decreased ROC-AUC of averaging the 10 largest ICAs compared to cumulative ICA using the SV approach. Those pixels may be reduced by using a vesselness filter, but interestingly, this problem did not occur with the MV approach (see Fig. 5; compare big avascular areas in B1 and C1).

Taking a distance approach with a fixed distance threshold still did not result in optimal discrimination between ischemic and nonischemic vasculature in OCTA images because OCTA in healthy retinae reveals varying vessel density as a function of distance to the fovea. We thus tested a distance-based approach with a threshold that is locally variable rather than a fixed threshold. This modification improved discrimination between healthy and ischemic vasculature but only for the SV approach. Using standardized norm curves is an established practice for other imaging procedures, such as retinal nerve fiber layer measurements to detect glaucoma. However, we need to consider that normative data can vary significantly between devices; Corvi et al.[25] demonstrated recently that seven different OCTA devices yielded significantly different measurements of the same eyes. Also, age-related physiological changes may influence the normative data, which were not specifically analyzed in our study.

Limitations and Future Applications

In conclusion, of the methods tested here, we found the distance-based detection of ICAs to be the most promising approach for quantification of retinal

ischemia. Further studies will be necessary to determine the value of this automated ischemia-quantification technique in everyday clinical practice. The approaches tested here with defined thresholding parameters were applied to OCTA scans from only one device; therefore, testing for device independency is necessary and requires prospective studies to compare distance-thresholded ICA analysis of same retinas scanned with different OCTA devices. Furthermore, our study is limited by the lack of comparisons between different diseases. A second study shortcoming is our rather small study population and its retrospective nature. Thus, a selection bias cannot be ruled out.

In the future, the distance approaches in particular should undergo further assessment to test (1) sensitivity and specificity at early disease stages and (2) the performance in retinae with macular edema, a frequent copathology in vascular diseases.

Acknowledgments

Disclosure: **P. Lauermann**, None; **C. van Oterendorp**, None; **M.W. Storch**, None; **M.H. Khattab**, None; **N. Feltgen**, None; **H. Hoerauf**, None; **S. Bemme**, None

References

1. Bertram B, Wolf S, Fiehöfer S, Schulte K, Arend O, Reim M. Retinal circulation times in diabetes mellitus type 1. *Brit J Ophthalmol*. 1991;75:462–465.
2. Hansen GL, Kofoed PK, Munch IC, et al. Retinal angiographic blood flowmetry is reduced in the ocular ischaemic syndrome. *Dan Med J*. 2013;60:A4716.
3. Hickam JB, Frayser R. A photographic method for measuring the mean retinal circulation time using fluorescein. *Invest Ophthalmol Vis Sci*. 1965;4:876–884.
4. Kim YJ, Jeong CB, Hwang J-M, Yang HK, Lee SH, Kim KG. New parametric imaging method with fluorescein angiograms for detecting areas of capillary nonperfusion. *J Healthc Inform Res*. 2014;20:191–198.
5. Or C, Sabrosa AS, Sorour O, Arya M, Waheed N. Use of OCTA, FA, and ultra-widefield imaging in quantifying retinal ischemia: a review. *Asia Pac J Ophthalmol (Phila)*. 2018;7:46–51.
6. Ha SO, Kim DY, Sohn CH, Lim KS. Anaphylaxis caused by intravenous fluorescein: clinical characteristics and review of literature. *Intern Emerg Med*. 2014;9:325–330.
7. Spaide RF, Fujimoto JG, Waheed NK. Optical coherence tomography angiography. *Retina*. 2015;35:2161–2162.
8. Yang S, Zhou M, Lu B, et al. Quantification of macular vascular density using optical coherence tomography angiography and its relationship with retinal thickness in myopic eyes of young adults. *J Ophthalmol*. 2017;2017:1397179.
9. Treder M, Lauermann JL, Alnawaiseh M, Heiduschka P, Eter N. Quantitative changes in flow density in patients with adult-onset foveomacular vitelliform dystrophy: an OCT angiography study. *Graefes Arch Clini Exp Ophthalmol*. 2018;256:23–28.
10. Samara WA, Shahlaee A, Adam MK, et al. Quantification of diabetic macular ischemia using optical coherence tomography angiography and its relationship with visual acuity. *Ophthalmology*. 2017;124:235–244.
11. Inooka D, Ueno S, Kominami T, et al. Quantification of macular microvascular changes in patients with retinitis pigmentosa using optical coherence tomography angiography. *Invest Ophthalmol Vis Sci*. 2018;59:433–438.
12. Shen C, Yan S, Du M, Zhao H, Shao L, Hu Y. Assessment of capillary dropout in the superficial retinal capillary plexus by optical coherence tomography angiography in the early stage of diabetic retinopathy. *BMC Ophthalmol*. 2018;18:217.
13. Jia Y, Bailey ST, Hwang TS, et al. Quantitative optical coherence tomography angiography of vascular abnormalities in the living human eye. *Proc Natl Acad Sci U S A*. 2015;112:E2395–E2402.
14. Gadde SGK, Anegondi N, Bhanushali D, et al. Quantification of vessel density in retinal optical coherence tomography angiography images using local fractal dimension. *Invest Ophthalmol Vis Sci*. 2016;57:246–252.
15. Durbin MK, An L, Shemonski ND, et al. Quantification of retinal microvascular density in optical coherence tomographic angiography images in diabetic retinopathy. *JAMA Ophthalmol*. 2017;135:370–376.
16. Zhang M, Hwang TS, Dongye C, Wilson DJ, Huang D, Jia Y. Automated quantification of nonperfusion in three retinal plexuses using projection-resolved optical coherence tomogra-

phy angiography in diabetic retinopathy. *Invest Ophthalmol Vis Sci*. 2016;57:5101–5106.
17. Hwang TS, Gao SS, Liu L, et al. Automated quantification of capillary nonperfusion using optical coherence tomography angiography in diabetic retinopathy. *JAMA Ophthalmol*. 2016; 134:367–373.
18. Schottenhamml J, Moult EM, Ploner S, et al. An automatic, intercapillary area-based algorithm for quantifying diabetes-related capillary dropout using optical coherence tomography angiography. *Retina*. 2016;36(suppl 1):S93–S101.
19. Shin JW, Sung KR, Lee JY, Kwon J, Seong M. Optical coherence tomography angiography vessel density mapping at various retinal layers in healthy and normal tension glaucoma eyes. *Graefes Arch Clini Exp Ophthalmol*. 2017;255: 1193–1202.
20. Lauermann JL, Eter N, Alten F. Optical coherence tomography angiography offers new insights into choriocapillaris perfusion. *Ophthalmologica*. 2018;239:74–84.
21. Zhang A, Zhang Q, Chen C-L, Wang RK. Methods and algorithms for optical coherence tomography-based angiography: a review and comparison. *J Biomed Opt*. 2015;20:100901.
22. Chu Z, Lin J, Gao C, et al. Quantitative assessment of the retinal microvasculature using optical coherence tomography angiography. *J Biomed Opt*. 2016;21:66008.
23. Lauermann JL, Treder M, Heiduschka P, Clemens CR, Eter N, Alten F. Impact of eye-tracking technology on OCT-angiography imaging quality in age-related macular degeneration. *Graefes Arch Clini Exp Ophthalmol*. 2017;255:1535–1542.
24. Hwang TS, Hagag AM, Wang J, et al. Automated quantification of nonperfusion areas in 3 vascular plexuses with optical coherence tomography angiography in eyes of patients with diabetes. *JAMA Ophthalmol*. 2018;136:929–936.
25. Corvi F, Pellegrini M, Erba S, Cozzi M, Staurenghi G, Giani A. Reproducibility of vessel density, fractal dimension, and foveal avascular zone using 7 different optical coherence tomography angiography devices. *Am J Ophthalmol*. 2018;186:25–31.